Classification of Very High Spatial Resolution Imagery Based on a New Pixel Shape Feature Set

Hua Zhang, Wenzhong Shi, Yunjia Wang, Ming Hao, and Zelang Miao

***Abstract*—This letter presents a novel spatial features extraction method for the high spatial resolution multispectral imagery (HSRMI) classification. First, Canny filter algorithm is applied to extract the edge information to obtain the fuzzy edge map. Secondly, adaptive threshold value for each pixel's homogeneous region (PHR) calculation is determined based on the fuzzy edge map and original image. Next, the PHR for every pixel is obtained based on the fuzzy edge map, adaptive threshold value and original image. And then, the pixel shape feature set (PSFS) is extracted based on the PHR. Lastly, SVM classifier is applied to classify the hybrid spectral and PSFS. Two different experiments were performed to evaluate the performance of PSFS, in comparison with spectral, gray level co-occurrence matrix (GLCM) and the existing pixel shape index (PSI). Experimental results indicate that the PSFS achieved the highest accuracy, hence, providing an effective spectral–spatial classification method for the HSRMI.**

***Index Terms*—Classification, high spatial resolution multispectral imagery (HSRMI), pixel shape feature set (PSFS), spatial feature extraction.**

I. Introduction

LAND cover information extraction from high spatial resolution multispectral imagery (HSRMI), such as IKONOS, QuickBird, and SPOT-5, is one of the widely used applications in the field of remotely sensed image classification. HSRMI provides more detailed ground information, while increasing in the spatial resolution always leads to reduction in the spectral statistical separability of different classes, namely, spectral similarity, which in turn involves high classification errors [1], [2]. The conventional pixel-wise classification methods only utilize spectral information regardless of spatial information, consequently are inadequate for HSRMI classification [3]. While HSRMI contains abundant spatial information concerning the shape, structure, and geometric feature can help for accurate interpretation. Thus, in recent years, many spectral–spatial classification methods, which integrate spectral with spatial characteristics, had been proved to be successful in enhancing the classification accuracy [4]–[7]. The grey level co-occurrence matrix (GLCM) is a widely spatial texture extraction method, and had been successfully used in many pattern recognitions of image [7]. Markov Random Field (MRF) is often used to improve the classification accuracy by incorporating spatial contextual information into classification [4]. A length–width extraction algorithm (LWEA) is developed to extract the length and width of spectral similar connected groups of pixels, and the LWEA is suitable for classifying the objects having different length–width ratio [5]. The structure information is extracted by applying the extended morphological profiles, and has been proved to be effective in HSRMI classification [6]. The pixel shape index (PSI) is introduced to provide the spatial features for classification [8]–[10], which extends direction-lines based on the spectral similarity to describe the structure of center pixel. The shape-size index (SSI) feature is extracted based on the homogeneous areas using spectral similarity between the center pixel and its neighbor pixels [11]. PSI and SSI had been proved to be useful in the classification of HSRMI to a certain extent. However, the thresholds are difficult to be determined and they are not appropriate for the concave objects such as the L-shape curve roads or building, as a result, uncertainty exits during the process of classification.

This letter presents a novel pixel shape feature set (PSFS) of the center pixel, which can provide multiple spatial information for enhancing the classification accuracy of HSRMI. The proposed approach was tested through two different experiments. The results demonstrated that the PSFS approach can achieve improved classification accuracy.

II. Pixel Shape Feature Set

In this section, we first define the pixel homogeneous region (PHR) based on spectral similarity between adjacent pixels. Then, on the basis of PHR, four pixel shape feature measures are proposed.

A. Pixel Homogeneous Region

To provide spatial features for enhancing classification accuracy, the pixel homogeneous region is calculated using the spectral similarity between the center pixel and its eight neighbor pixels. PHR is defined by the following methods:

1) Edge Detection:

$$\text{edge}(i) = \frac{1}{N}\sum_{d=1}^{N}\text{edge}_d(i) \tag{1}$$

Manuscript received May 17, 2013; revised July 8, 2013 and August 21, 2013; accepted September 14, 2013. Date of publication October 10, 2013; date of current version December 11, 2013. This work was supported by the National Natural Science Foundation of China under Grants 41201451, 41331175, and 51174287, the Fundamental Research Funds for the Central Universities under Grant 2010QNB13, and a Project Funded by the Priority Academic Program Development of Jiangsu Higher Education Institutions.

H. Zhang, Y. Wang, and M. Hao are with the Key Laboratory for Land Environment and Disaster Monitoring of State Bureau of Surveying and Mapping (SBSM), China University of Mining and Technology, Xuzhou 221116, China (e-mail: zhhuamesi@gmail.com; wyj4139@163.com; haomingcumt@gmail.com).

W. Shi and Z. Miao are with the Department of Land Surveying and GeoInformatics, The Hong Kong Polytechnic University, Kowloon, Hong Kong (e-mail: lswzshi@polyu.edu.hk; cumtzlmiao@gmail.com).

Color versions of one or more of the figures in this paper are available online at http://ieeexplore.ieee.org.

Digital Object Identifier 10.1109/LGRS.2013.2282469

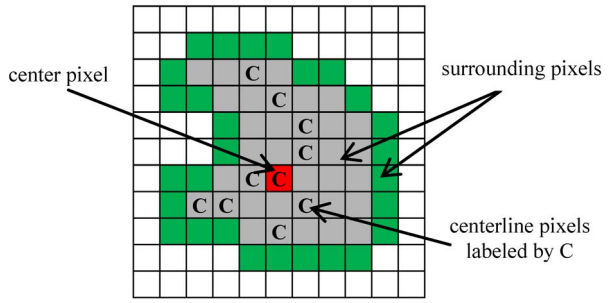

Fig. 1. Pixel homogeneous region.

where edge(i) denotes an estimated probability value which represents the likelihood of ith pixel belonging to an edge pixel, N is the number of spectral bands, edge$_d(i)$ indicates whether the ith pixel is an edge pixel or not in band d, if edge$_d(i) = 1$, then the ith pixel is an edge pixel, if edge$_d(i) = 0$, then the ith pixel is not an edge pixel. Here, edge$_{\rm d}(i)$ is obtained through the Canny filter algorithm.

2) Calculating the Spectral Similarity:

$$\mathrm{PH}(i) = \arg\min_{x \in X} (1 + \mathrm{edge}(i)) \sum_{d=1}^{N} |P_d(i) - P_d(x)| \quad (2)$$

where PH(i) represents the spectral similarity between the ith pixel (center pixel) and its surrounding pixels. $P_d(i)$ and $P_d(x)$ denotes the center pixel spectral value and its neighbor pixel spectral value in band d, respectively. X denotes the set of eight neighbor pixels. It can be inferred from (2), when the value of edge$_{\rm d}(i)$ increases, the likelihood that the pixel locates in the homogeneous region will become smaller.

3) Generating PHR: Supposing a threshold T, if PH$(i) \leq T$, then the closed neighbor pixel is thought to be contained in the same object as the center pixel located in, then it will be merged into the center pixel, a new center pixel is produced, and the spectral value of new center pixel is calculated by

$$P_d^{n+1}(i) = \frac{nP_d^{(n)}(i) + P_d(c)}{n+1} \quad (3)$$

where n is the number of previous center pixel, $P_d^{n+1}(i)$ denotes the new produced center pixel value, $P_d^n(i)$ is the value of the nth center pixel in band d, and $P_d(c)$ is the closest neighbor pixel value.

Repeating step 2) and 3) until no more new neighbor pixels can be merged into the center pixel, the PHR of one pixel is produced (Fig. 1). As shown in Fig. 1, the red pixel is the center pixel, the grey, red and green pixels compose the PHR of the center pixel. PHR for each pixel in the entire image will be obtained to calculate the pixel shape feature set (PSFS) for every pixel by the proposed methods in the letter.

B. Adaptive Threshold Value

In the process of obtaining the PHR, how to determine the threshold T becomes important and difficult. There is no better method for determining the optimum threshold, and the threshold is commonly determined manually, as a result, uncertainty exists in the result. In this letter, an adaptive threshold method is provided based on the image edge pixels information.

In essence, the edge pixels of image can characterize the local discontinuity of the entire image, and can approximately represent the whole image characteristics. Therefore, the edge pixels here are used to obtain the optimal threshold values, the threshold calculation can be defined as

$$T(i) = \sum_{d=1}^{N} \left| P_d(i) - \frac{1}{M_d} \sum_{k=1}^{M_d} X_d(k) \right| \quad (4)$$

where $T(i)$ is the threshold value for obtaining the PHR of ith pixel used in Section A, M_d is the number of edge pixels in band d, $X_d(k)$ denotes the spectral value of edge pixel in band d. Here, the edge pixels are obtained through the Canny filter algorithm based on all bands in the image.

C. Pixel Shape Feature Set

On the basis of PHR, PSFS of the center pixel, including PAI, LW, Solidity and Extend measures, will be calculated.

1) LW:

$$\mathrm{LW} = P_{\mathrm{Length}}/P_{\mathrm{Width}}$$
$$P_{\mathrm{Width}} = P_{\mathrm{Area}}/P_{\mathrm{Length}} \quad (5)$$

where LW represents the narrow degree of the center pixel in the PHR. P_{Length} denotes the length of centerline of PHR, P_{Width} denotes the width of PHR, P_{Area} is the amount of pixels in the PHR. As shown in Fig. 1, P_{Length} can be determined by counting the number of pixels labeled by C, and P_{Area} can be got by counting the number of the green, grey and red pixels. The LW is useful for identifying narrow objects from those objects with the similar area, such as identifying roads from buildings, especially suitable for the curve road identification.

2) PAI:

$$\mathrm{PAI} = P_{\mathrm{Perimeter}}/P_{\mathrm{Area}} \quad (6)$$

where PAI (Perimeter Area Index) represents the shape and size of the center pixel in the PHR. $P_{\mathrm{Perimeter}}$ is the length of the boundary of the PHR, P_{Area} is the amount of pixels in the PHR. As shown in Fig. 1, $P_{\mathrm{Perimeter}}$ can be determined by counting the number of the green pixels. $P_{\mathrm{Perimeter}}$ and P_{Area} describes shape and size of the PHR, respectively. As is described above, the LW is useful for identifying narrow objects from those objects having the similar area, but it is not suitable for regions which have similar LW. For example, those regions including roads and buildings which have the similar LW, from (6), if these regions have the similar P_{Area}, road is generally narrower than building, the $P_{\mathrm{Perimeter}}$ of road is bigger than that of the building, therefore, PAI of these objects are different, and can be used to improve these objects classification accuracies. PAI is very useful for improving the classification of spectral similarity and LW objects such as water-shadow and building-road.

3) Solidity:

$$\mathrm{Solidity} = P_{\mathrm{Area}}/P_{\mathrm{ConvexArea}} \quad (7)$$

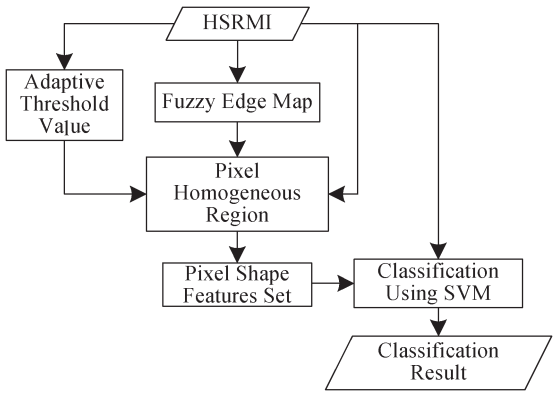

Fig. 2. Flowchart of the proposed classification algorithm procedure.

where Solidity indicates substantial degree of the center pixel in the PHR, $P_{\mathrm{ConvexArea}}$ is the number of pixels in the convex hull of PHR, the smaller Solidity means the greater degree of complexity. Supposing a curve road pixels group has the same area of a building pixels group, the Solidity value of the former is smaller than the latter, and the same law can be drawn from the group of tree, grass, etc. The Solidity is always used to identify the nonrectangular objects.

4) Extent:

$$\text{Extent} = P_{\mathrm{Area}}/P_{\mathrm{Bounding\ Box\ Area}} \tag{8}$$

where Extent describes extension degree of the center pixel in the PHR, $P_{\mathrm{BoundingBoxArea}}$ is the number of pixels in the bounding box of PHR, the smaller Extent means the greater degree of complexity. Supposing a curve road pixels group has the same area of a building pixels group, the Extent value of the former is smaller than the latter, and the same law can be drawn from the group of tree, grass, etc. The Extent is always used to identify the regular objects.

The contributions of PSFS are as follows: 1) edge pixels are considered; 2) adaptive threshold value for obtaining PHR; 3) multiple shape features at an unfixed window.

III. SVM-Based Classification Integrating Spectral Information and Pixel Shape Feature Set

In this letter, SVM classifier is performed to classify the image based on the spectral feature and extracted PSFS. The flowchart of proposed methods is shown in Fig. 2. Given a high spatial resolution multispectral image. First, the Canny filter algorithm is used to extract the edge information to obtain the fuzzy edge map. Second, adaptive threshold value for calculating each pixel's PHR is determined based on the filtered maps by the Canny filter algorithm and original image. Next, PHR for every pixel is obtained based on the fuzzy edge map, the adaptive threshold value and original image, and the PSFS is extracted based on PHR. Last, the SVM classifier is applied to classify the image by integrating spectral with PSFS.

The implementation of proposed classification method includes the following five steps:

Step 1—Obtaining Fuzzy Edge Map: To avoid the disturbance of small artefacts while minimizing the variation of the original image and preserving the edge information, the median filter is firstly performed to the image using a 3-by-3 neighborhood. Then, the Canny filter algorithm is used to obtain the edge information based on the filtered image, and several binary maps are produced for all bands, the value of $\mathrm{edge}_d(i)$ is got. Last, (1) is used to calculate $\mathrm{edge}(i)$ to obtain the fuzzy edge map.

Step 2—Computation of Adaptive Threshold Value: Based on the obtained edge pixels maps through the Canny filter algorithm and the original image, (4) is used to calculate the threshold $T(i)$ for each pixel to obtain the PHR.

Step 3—Obtaining Pixel Homogeneous Region: On the basis of fuzzy edge map, adaptive threshold value and original image, the PHR of every pixel is obtained using the method proposed in Section II-A.

Step 4—Extracting Pixel Shape Feature Set: The PSFS including PAI, LW, Solidity and Extent measure, is extracted based on the PHR using the methods proposed in Section II-C.

Step 5—Classification Based on SVM: The extracted PSFS and multiple spectral features are all normalized into [0, 1], here, the extracted features are treated as four bands and integrated with the multiple spectral features. The SVM classifier is performed to classify the integrated features image.

IV. Experimental Results And Discussion

The proposed classification algorithms are based on the widely used SVM library LIBSVM [10] in Matlab7.8. Two experiments were conducted to test the performance. Comparisons were made between the classification based on spectral features alone, spectral information with GLCM and PSI [6] and PSFS spatial features. The GLCM features include Homogeneity, Contrast, Angular Second Moment and Entropy, and the window sizes for GLCM is optimized from 3×3 to 27×27 window size to make a fair comparison. The image covers water, grass, tree, building, road, bare soil and shadow classes. Reference data are obtained through visual interpretation method based on the well rectified image. For the SVM, The all extracted spatial features and multiple spectral features are normalized into [0, 1], Training samples are selected automatically by using the stratified random sampling method based on the reference data, and the remains of reference data are treated as the test samples. RBF kernel is used and the multiclass SVM is applying by the one-against-one (OAO) method. Penalty Parameter (c) and Gamma in the RBF (γ) is obtained by the Grid-Search method [12]. Producer's Accuracy, Overall Accuracy and Kappa Coefficient based on the confusion matrix are used to evaluate the classification performances of the four algorithms [13].

A. Experiment 1: QuickBird Image of Xuzhou Suburb Area

In experiment 1, a 0.61-m resolution QuickBird (512×512 pixels) containing three multispectral bands (RGB) of the suburb area of Xuzhou, China, which was acquired on August 2005 [Fig. 3(a)] was used. Fig. 3(b) shows the reference data. Table I describes the training and testing samples in the experiment 1. Fig. 3(c) and (d) shows the spatial distribution of the training and testing samples, respectively. Two parameters c

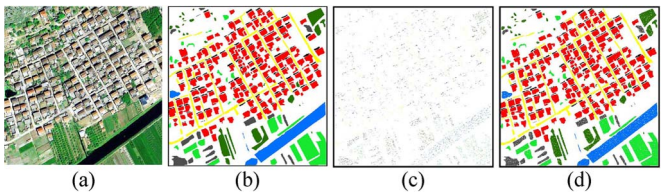

Fig. 3. (a) QuickBird image of the suburb of Xuzhou; (b) Reference data; (c) training data; (d) testing data. Blue (water). (Light green) Grass. (Dark green) tree. (Red) Building. (Yellow). Road. (Gray) Bare soil. (Black) Shadow.

TABLE I
NUMBER OF SAMPLES, PRODUCER'S ACCURACY, OVERALL ACCURACY AND KAPPA COEFFICIENT OF CLASSIFICATION IN EXPERIMENT 1

Class	Number of Training samples	Number of Testing samples	Spectral	GLCM (17×17)	GLCM (19×19)	GLCM (21×21)	PSI	PSFS
Water	526	9683	90.81%	98.76%	98.62%	98.44%	98.85%	99.30%
Grass	532	12759	75.64%	93.49%	93.88%	93.71%	92.23%	93.06%
Tree	531	8237	75.94%	89.64%	89.86%	90.92%	87.68%	92.08%
Building	530	44904	58.25%	70.50%	71.68%	71.53%	82.31%	84.94%
Road	522	11654	83.60%	81.83%	79.35%	79.08%	83.14%	86.12%
Bare soil	543	4900	89.10%	93.57%	94.82%	95.00%	92.33%	93.71%
Shadow	491	4421	82.24%	97.69%	98.10%	97.96%	95.32%	98.62%
Overall Accuracy			71.05%	81.79%	82.17%	82.13%	86.94%	89.28%
Kappa Coefficient			0.6362	0.7640	0.7681	0.7674	0.8268	0.8570

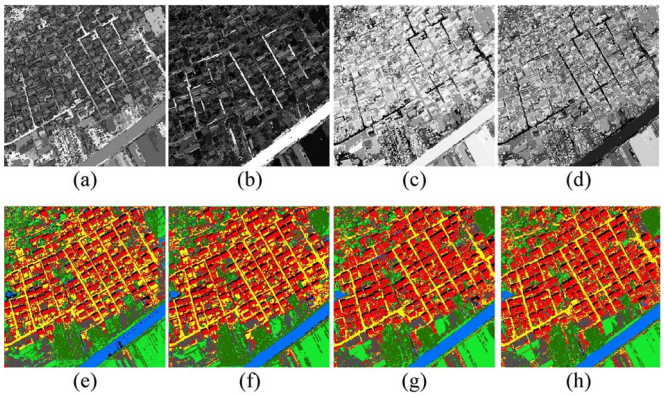

Fig. 4. (a)–(d) is pixel shape feature image based on PAI, LW, Solidity and Extent, respectively; (e)–(h) is the classification maps based on Spectral, GLCM (19 × 19), PSI and PSFS, respectively in experiment 1. Blue (water). (Light green) Grass. (Dark green) tree. (Red) Building. (Yellow). Road. (Gray) Bare soil. (Black) Shadow.

and γ of SVM for spectral features alone, spectral information with GLCM (19×19) and PSI and PSFS features were 16, 4 and 16, 16 and 4, 8 and 32, 4, respectively. The parameters for the PSI were set as: $D = 20$, $T_1 = 110$, $T_2 = 60$.

Fig. 4(a)–(d) shows the PAI, LW, Solidity and Extent shape features maps extracted from the image, respectively. Fig. 4(e)–(h) shows the classification results derived from the spectral, GLCM (19 × 19), PSI and PSFS, respectively. In addition, the GLCM (19 × 19) achieved the highest classification accuracy using different window sizes, Fig. 4 only presents the result of GLCM (19 × 19). As shown in Fig. 4(a)–(d), different object shapes were described by the four shape features. Seen from Fig. 4(e), water and shadow, road and building and bare soil, tree and grass were confused in the map due to their spectral similarity. Considering the spatial information in the classification, Fig. 4(f)–(h) all give more homogenous regions than Fig. 4(e). PSFS gives a more satisfactory classification result than GLCM and PSI, the reason is partly that the GLCM

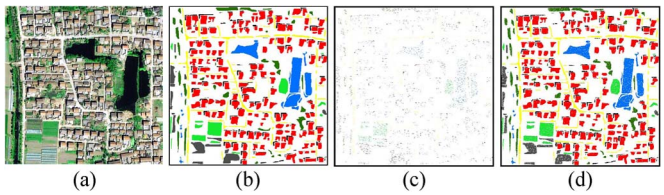

Fig. 5. (a) QuickBird image of the urban center of Xuzhou; (b) Reference data; (c) training data; (d) testing data. Blue (water). (Light green) Grass. (Dark green) tree. (Red) Building. (Yellow). Road. (Gray) Bare soil. (Black) Shadow.

TABLE II
NUMBER OF SAMPLES, PRODUCER'S ACCURACY, OVERALL ACCURACY AND KAPPA COEFFICIENT OF CLASSIFICATION IN EXPERIMENT 2

Class	Number of Training samples	Number of Testing samples	Spectral	GLCM (19×19)	GLCM (21×21)	GLCM (23×23)	PSI	PSFS
Water	570	9482	95.98%	94.00%	97.48%	97.99%	99.62%	99.85%
Grass	523	4711	76.97%	87.12%	85.97%	85.63%	93.57%	96.67%
Tree	578	6198	80.01%	86.11%	85.35%	83.74%	91.48%	94.09%
Building	600	38629	80.31%	79.40%	85.48%	81.41%	88.06%	92.73%
Road	561	8756	93.14%	91.96%	91.38%	93.71%	94.10%	95.24%
Bare soil	565	5087	93.57%	93.47%	94.40%	94.95%	95.34%	98.29%
Shadow	575	5095	84.22%	87.07%	93.74%	96.55%	98.31%	98.82%
Overall Accuracy			84.55%	85.01%	88.75%	87.12%	91.90%	94.98%
Kappa Coefficient			0.7921	0.7987	0.8464	0.8263	0.8888	0.9304

features were extracted at a fixed window without considering the different shapes for objects and the PSI only uses the direction-lines which is not appropriate for the concave regions, while PSFS can adequately describe different objects using multiple shape features at an unfixed window. Table I lists the comparisons between Producer accuracy, Overall Accuracy and Kappa Coefficient of spectral, GLCM, PSI and PSFS. Seen from Table I, because the spatial contexture information is considered in GLCM, PSI and PSFS, they all yield accuracies than spectral feature alone. The PSFS using multiple shape features gives the best Overall Accuracy and the best class producer's accuracies. Compared with spectral, GLCM (19 × 19) and PSI, the improvement for PSFS in Overall Accuracy is about 18.21%, 7.11% and 2.33%, respectively. According to the results of McNemar's test, PSFS between the spectral, GLCM (19 × 19), PSI and PSFS classification accuracies are all statistically significant at the 5% level of significance. [14].

B. Experiment 2: QuickBird Image of Xuzhou Urban Center Area

In experiment 2, another 0.61-m resolution QuickBird (512 × 512 pixels) containing three multispectral bands (RGB) of the urban center area of Xuzhou, China, which was acquired on August, 2005 [Fig. 5(a)] was used. Fig. 5(b) shows the reference data. Table II describes the training and testing samples in the experiment 2. Fig. 5(c) and (d) shows the spatial distribution of the training and testing samples, respectively. Two parameters c and γ of SVM for spectral features alone, spectral information with GLCM (21 × 21) and PSI and PSFS spatial features were 8, 32 and 16, 8 and 4, 8 and 8, 8, respectively. The parameters for the PSI were set as: $D = 20$, $T_1 = 120$, $T_2 = 60$.

Fig. 6(e)–(h) shows the classification maps derived from the spectral, GLCM (21 × 21), PSI and PSFS, respectively. In addition, the GLCM (21 × 21) got the highest classification

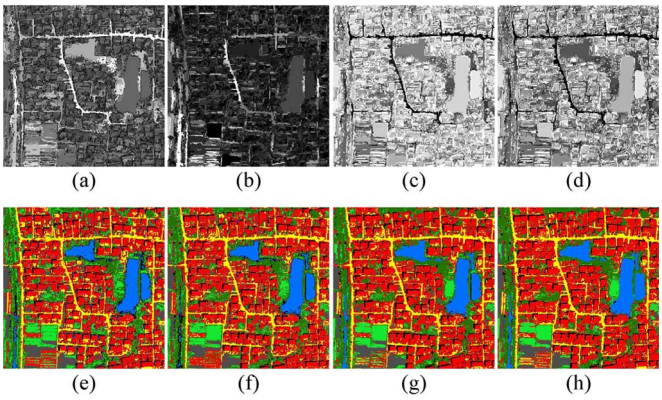

Fig. 6. (a)–(d) is pixel shape feature image based on PAI, LW, Solidity and Extent, respectively; (e)–(h) is the classification maps based on Spectral, GLCM (21 × 21), PSI and PSFS, respectively in experiment 2. Blue (water). (Light green) Grass. (Dark green) tree. (Red) Building. (Yellow). Road. (Gray) Bare soil. (Black) Shadow.

accuracy using different window sizes, Fig. 6 only shows the result of GLCM (21 × 21). As shown in Fig. 6(a)–(d), different objects' shapes were described by the four shape features. Seen from Fig. 6(e), because the spectral features were used alone, water and shadow, road and building, and bare soil, tree, and grass were confused in the map. Fig. 6(f)–(h) all give more homogenous regions than Fig. 6(e). PSFS gives a more satisfactory result than GLCM and PSI. The reason is partly that the GLCM texture features were extracted at a fixed window and PSI only using he direction-lines statistic features, while PSFS can adequately describe different objects using multiple shape features at an unfixed window. Table II lists the comparisons between Producer Accuracy, Overall Accuracy and Kappa Coefficient of spectral, GLCM, PSI and PSFS. Seen from Table II, because the spatial contexture information is considered in GLCM, PSI and PSFS, they all yield higher classification accuracies than spectral. The PSFS gives the best Overall Accuracy and the best class producer's accuracies. Compared with spectral, GLCM (21 × 21) and PSI, the improvement for PSFS in Overall Accuracy is about 10.43%, 6.23% and 3.08%, respectively. According to the results of McNemar's test, PSFS between the spectral, GLCM (21 × 21), PSI and PSFS classification accuracies are all statistically significant at the 5% level of significance.

Above all, from two different experiments, we can deduce that the PSFS achieved the highest Producer's Accuracy, Overall Accuracy, and Kappa Coefficient. While the accuracies were improved more in experiment 1 than that in experiment 2, the reason is that the objects are more regular in experiment 1 than that in experiment 2. PSFS is especially suitable for the regularized and complex objects classification.

V. Conclusion

A novel PSFS algorithm for spectral–spatial classification of HSRMI had been presented in this letter. First, the fuzzy edge map was produced by applying the Canny filter algorithm on the image, and then the adaptive threshold value for each pixel was calculated based on edge maps and original image. Secondly, PHR for every pixel was obtained based on the fuzzy edge map, the adaptive threshold value and original image. Thirdly, based on the PHR, PSFS was extracted. Lastly, the spectral and PSFS features were normalized and fused to classification based on SVM. Two different experiments were carried out to evaluate the performance of the PSFS. Compared with spectral, GLCM and PSI, the PSFS achieves the highest enhancements in both the classification accuracy and visual interpretation. These evince that the PSFS is an effective algorithm for HSRMI. Due to the complexity of objects in the image, we can use a multiple shape feature set which can characterize the object from different points to enhance the classification accuracy.

In our future work, more work will be carried on methods of determining the optimal threshold, and the PSFS will be applied in other type remotely sensed images and others.

References

[1] Q. Yu, P. Gong, N. Clinton, G. Biging, M. Kelly, and D. Schirokauer, "Object-based detailed vegetation classification with airborne high spatial resolution remote sensing imagery," *Photogramm. Eng. Remote Sens.*, vol. 72, no. 7, pp. 799–811, Jul. 2006.

[2] L. Bruzzone and L. Carlin, "A multilevel context-based system for classification of very high spatial resolution images," *IEEE Trans. Geosci. Remote Sens.*, vol. 44, no. 9, pp. 2587–2600, Sep. 2006.

[3] D. A. Landgrebe, *Signal Theory Methods in Multispectral Remote Sensing*. New York, NY, USA: Wiley, 2003.

[4] Y. Tarabalka, M. Fauvel, and J. Chanussot, "SVM- and MRF-based method for accurate classification of hyperspectral images," *IEEE Geosci. Remote Sens. Lett.*, vol. 7, no. 4, pp. 736–740, Oct. 2010.

[5] A. K. Shackelford and C. H. Davis, "A hierarchical fuzzy classification approach for high-resolution multispectral data over urban areas," *IEEE Trans. Geosci. Remote Sens.*, vol. 41, no. 9, pp. 1920–1932, Sep. 2003.

[6] J. A. Benediktsson, M. Pesaresi, and K. Arnason, "Classification and feature extraction for remote sensing images from urban areas based on morphological transformations," *IEEE Trans. Geosci. Remote Sens.*, vol. 41, no. 9, pp. 1940–1949, Sep. 2003.

[7] A. Baraldi and F. Parmiggiani, "An investigation of the textural characteristics associated with grey level co-occurrence matrix statistical parameters," *IEEE Trans. Geosci. Remote Sens.*, vol. 33, no. 2, pp. 293–304, Mar. 1995.

[8] L. Zhang, X. Huang, B. Huang, and P. Li, "A pixel shape index coupled with spectral information for classification of high spatial resolution remotely sensed imagery," *IEEE Trans. Geosci. Remote Sens.*, vol. 44, no. 10, pp. 2950–2961, Oct. 2006.

[9] X. Huang, L. Zhang, and P. Li, "Classification and extraction of spatial features in urban areas using high-resolution multispectral imagery," *IEEE Geosci. Remote Sens. Lett.*, vol. 4, no. 2, pp. 260–264, Apr. 2007.

[10] X. Huang, L. Zhang, and P. Li, "Classification of very high spatial resolution imagery based on the fusion of edge and multispectral information," *Photogramm. Eng. Remote Sens.*, vol. 74, no. 12, pp. 1585–1596, Dec. 2008.

[11] Y. Han, H. Kim, J. Choi, and Y. Kim, "A shape–size index extraction for classification of high resolution multispectral satellite images," *Int. J. Remote Sens.*, vol. 33, no. 6, pp. 1682–1700, Mar. 2008.

[12] C. C. Chang and C. J. Lin, "LIBSVM: A library for support vector machines," 2001. [Online]. Available: http://www.csie.ntu.edu.tw/~cjlin/libsvm/

[13] R. G. Congalton, R. G. Oderwald, and R. A. Mead, "Assessing landsat classification accuracy using discrete multivariate statistical techniques," *Photogramm. Eng. Remote Sens.*, vol. 49, no. 12, pp. 1671–1678, Dec. 1983.

[14] G. M. Foody, "Thematic map comparison evaluating the statistical significance of differences in classification accuracy," *Photogramm. Eng. Remote Sens.*, vol. 70, no. 5, pp. 627–633, May 2004.